Quantifying small molecule phenotypic effects using mitochondrial morpho-functional fingerprinting and machine learning

Supplementary information

Lionel Blanchet[1,2,3,4], Jan A.M. Smeitink[3,4,5], Sjenet E. van Emst - de Vries[1,4], Caroline Vogels[4], Mina Pellegrini[4], An I. Jonckheere[5], Richard J.T. Rodenburg[3,5], Lutgarde M.C. Buydens[2,3],
Julien Beyrath[4], Peter H.G.M. Willems[1,3,4] and Werner J.H. Koopman[1,3,4,*]

[1]Department of Biochemistry, Radboud Institute for Molecular Life Sciences, Radboud University Medical Center, P.O. Box 9101, NL-6500 HB Nijmegen, The Netherlands
[2]Analytical Chemistry/Chemometrics, Institute for Molecules and Materials, Radboud University, postvak 61, P.O. Box 9010, 6500 GL Nijmegen, The Netherlands.
[3]Centre for Systems Biology and Bioenergetics, Radboud University Medical Center, Nijmegen, The Netherlands. [4]Khondrion BV, P.O. Box 9101, NL-6500 HB Nijmegen, The Netherlands.
[5]Department of Pediatrics, Nijmegen Centre for Mitochondrial Disorders, Radboud University Medical Center, Nijmegen, Geert Grooteplein 10, PO BOX 9101, 6500 HB Nijmegen, The Netherlands.

[*]**Correspondence**: Dr. W.J.H. Koopman, 286 Biochemistry, Radboud Institute for Molecular Life Sciences (RIMLS), Radboud University Medical Centre (RUMC), P.O. Box 9101, NL-6500 HB Nijmegen, The Netherlands, Tel: +31-24-3614589, Fax: +31-24-3616413, E-mail: w.koopman@ncmls.ru.nl

Key words: high-content microscopy, TMRM, mitochondrial morphology, antioxidants.

1. SUPPLEMENTARY MATERIALS AND METHODS

Cell lines and culture conditions **-** Primary human skin fibroblasts were obtained from healthy individuals (CT5118, CT5119, CT5120) and various LS patients (P) with isolated mitochondrial complex I (CI) deficiency (OMIM 252010) that were previously characterized at the genetic, biochemical and cellular level.[1–4] Patient cell lines included P5866 (*NDUFV1* mutation), P6173 (*NDUFS1* mutation), P5067 (*NDUFS2* mutation), P5260 (*NDUFS4* mutation), P5175 (*NDUFS7* mutation), P7206 (*NDUFS7* mutation) and P6603 (*NDUFS8* mutation). In all patient cells CI deficiency was biochemically confirmed in muscle tissue and cultured skin fibroblasts. Biopsies were performed following informed parental consent and according to the relevant Institutional Review Boards. Cells were cultured in Medium 199 (M199; #22340-020; Invitrogen, Breda, The Netherlands) in a humidified atmosphere (95% air, 5% CO_2) at 37^o C. The culture medium contained Earle's salts, 25 mM HEPES, 5.5 mM D-glucose, 0.7 mM L-glutamine, 10% (v/v) fetal calf serum, 100 IU/ml penicillin and 100 IU/ml streptomycin. None of the treatments described in this study induced cell detachment from the glass-bottom or visual signs of cell death.

Microscopy imaging of mitochondrial morphology and membrane potential **-** Routinely, fibroblasts were incubated in Medium 199 (M199) containing 100 nM tetramethyl rhodamine methyl ester (TMRM; Invitrogen) for 25 min at 37^{o}C. Next, cells were washed with PBS and coverslips were mounted in a temperature-controlled chamber attached to the stage of an inverted microscope (AxioObserver Z1; Carl Zeiss, Jena, Germany) equipped with Plan-Apochromat oil immersion objectives (40x/1.3 and 63x/1.40). TMRM was used in non-quenching mode.[5] During measurements, cells were placed in a HEPES–Tris (HT) solution (pH 7.4 adjusted with Tris, 132 mM NaCl, 4.2 mM KCl, 5.5 mM D-glucose, 1 mM $MgCl_2$, 1 mM $CaCl_2$, 10 mM HEPES). TMRM was excited at 540 nm using a monochromator (Polychrome 5000; TILL Photonics, Gräfelfing, Germany), and fluorescence light was directed by a 560DRLP dichroic mirror (Omega Optical, Brattleboro,VT, USA) through a 565ALP emission filter (Omega) onto a CoolSNAP HQ2 monochrome CCD-camera (Roper Scientific Photometrics, Evry Cedex, France). Hardware was controlled using Metafluor 7.0 software (Molecular Devices Corporation, Downingtown, PA, USA).

Validation of the TMRM-based staining and image quantification protocol – Various quantitative parameters describing mitochondrial morphology and TMRM intensity ("morpho-functional descriptors") were extracted from the microscopy images by applying an automated image processing and analysis algorithm. This strategy was extensively validated previously in primary human skin fibroblasts from healthy individuals and LS patient cells.[1,4–12] In brief, a background corrected image (Fig. 1: COR) is generated from each microscopy image (RAW) that is subsequently contrast optimized (LCS), processed by a top-hat filter (THF), median filtered (MED) and thresholded to obtain a binary image (BIN). The latter image depicts white mitochondrial object on a black background. Next, the COR and BIN images are combined using a Boolean AND operation to obtain a masked image (MSK) from which the morpho-functional descriptors are calculated. For visualization purposes, a look-up table (LUT) can be used for color-coding the TMRM fluorescence intensity in the image (LUT).

Quantification of cellular reactive oxygen species (ROS) levels **–** Cells were cultured in M199 up to 70-80% confluence. Cells were then seeded in black 96 well plates (BD Falcon; #353219; **Becton Dickinson, Erembodegem, Belgium**) and treated with vehicle (0.1% DMSO) or test compound for 72 hours. Next, cells were stained with the ROS-sensing reporter molecules 5-(and-6)-chloromethyl-2',7'-dichlorodihydro-fluorescein (CM-H_2DCFDA; **Invitrogen**; 1 µM in HT solution during 10 min at

RT in the dark) or hydroethidium (HEt; **Invitrogen**; 10 µM in HT solution during 10 min at RT in the dark), washed and cell images were acquired on a BD Pathway 855 microscope using a x20 objective (**Becton Dickinson**). CM-H_2DCFDA-stained cells were visualized using a 488d10 excitation filter, a Fura/FITC dichroic mirror and a 515LP emission filter. HEt-stained cells were visualized using 488d10 excitation filter, a Fura/FITC dichroic mirror and a 570LP emission filter.

ORAC assay - The oxygen radical absorbance capacity (ORAC) assay is based on the scavenging of peroxyl radicals generated by AAPH (2,2'-azobis-2-methyl-propanimidamide, dihydrochloride), which prevents degradation of fluorescein and its loss of fluorescence. The ORAC assay was carried out using 96-well plates and a FluoStar Omega plate reader (BMG Labtech, Ortenberg, Germany). Different dilutions of the antioxidant Trolox (400 µM - 12.5 µM; used as a standard) and the to-be-tested compounds were freshly prepared in phosphate buffer (10 mM, pH 7.4). Aliquots (25 µl) of the test compounds were added to individual wells that contained 150 µl of fluorescein (10 nM in phosphate buffer). Following pre-incubation (30 min, 37˚ C), the background fluorescence signal was determined (90 s interval; 4 cycles in total) using a 485 nm excitation and 520 nm emission wavelength. After this, 25 µl (240 mM) of AAPH was injected using the on-board injector system and fluorescence measurements were continued up to 90 min. Numerical data was analyzed using the MARS software (BMG Labtech). From the normalized curves, the area under the fluorescence decay curve (AUC) was calculated. The net AUC was then plotted as a function of compound concentration and a linear fit was performed to calculate the slope of the curve. For each sample the slope was normalized to that of Trolox yielding Trolox Equivalent (TE) values. During curve fitting, we used Pearson's correlation coefficient R (or product moment correlation coefficient) as an estimate of the population correlation coefficient. Values of -1 and +1 indicate a perfect linear relationship between the two variables.[13]

Machine learning strategy - Following extraction of morpho-functional descriptor variables from the images, outliers can be detected and removed from each individual image in a multivariate way. To this end we used robust principal component analysis and automatic determination of the cut-off values based upon Hotelling's T^2 distribution and Q^2. Next, the resulting set of descriptor variables was condensed by calculating the median value for each descriptor for every image, resulting in 31 descriptor values (features) per image. The meaning of various descriptors is provided in Supplementary Table S1. To allow optimal pattern recognition and image classification, a training algorithm was used to recognize a specific multivariate pattern. This pattern must allow separating the two classes of fibroblasts from a healthy subject (CT5120) and a patient with isolated complex I (CI) deficiency (P5175). To evaluate the training algorithm, the available data is divided into "training" and "test" sets. The training set is used to construct the multivariate classification models, whereas the test set is used to assess their predictive performance. We compared the performance of five classification models: Logistic Regression (LogReg), Linear Discriminant Analysis (LDA), Partial Least Squares Discriminant Analysis (PLSDA), Quadratic Determinant Analysis (QDA) and Support Vector Machines (SVMs). LogReg, LDA and PLSDA assume that the separation between the two cell lines can be obtained using a linear combination of the descriptor variables. In contrast, QDA and SVMs do not make this assumption and are therefore are able to detect non-linear separation. Most of these methods can be used directly without settings any parameters. The required optimization of the number of latent variables in PLSDA was done by cross validation. Using SVMs requires choosing a kernel. Here we applied the radial basis function. The optimal width (sigma) of the Gaussian used in this kernel was found to be equal to 30 when using the original data and 3 when using the distribution parameters. For each model, its classification performance was evaluated using the test set. Next, the classification model was applied either on the complete dataset (*i.e.* each value for each descriptor for

each mitochondrial object in each image was used), the mean per cell dataset (*i.e.* the mean value for each descriptor in each image) or the median per cell dataset (*i.e.* the median value for each descriptor in each image). Below, each of the five models is briefly described:

1. Logistic regression - Logistic regression[14] ("LogReg") belongs to the family of generalized linear models. The observed descriptors are linked to a (binary) response y, corresponding in this study to the type of cell: patient or control. The probability a given cell to be from a patient ($\hat{y}$) cell line is evaluated using all the morphological descriptors (x_1,x_2,…x_p). The model can be described by the following equation, where β_0 represents the intercept of the model and the coefficients β_1 to β_p the regression coefficients of x_1 to x_p respectively:

$$\hat{y} = \beta_0 + \beta_1 x_1 + \beta_2 x_2 + ... + \beta_p x_p \qquad \textbf{(Equation 1)}$$

Each of the regression coefficients represents the relative importance of the corresponding descriptor in the model. In our case, positive regression coefficients increase the probability to be classified as control, negative regression coefficients lower it. The previous equation can also be written in a more concise manner using matrix notation:

$$x = [x_1, x_2, ...x_p] \qquad \textbf{(Equation 2)}$$

$$\beta = [\beta_1, \beta_2, ...\beta_p] \qquad \textbf{(Equation 3)}$$

$$\hat{y} = \beta_0 + \beta x \qquad \textbf{(Equation 4)}$$

LogReg is known to require a relatively large sample size. In general, the number of samples should be 10 times greater than the number of variables.[15] This criterion is met in the current study where 31 descriptors (variables) were extracted from 1000 images (samples).

2. Linear Discriminant Analysis - Linear Discriminant analysis[14,16] (LDA) is another supervised analysis method aiming to discriminate between two groups of samples using a set of descriptors. The main assumption of LDA is that the groups of samples are following multivariate Gaussian distribution and have common covariance matrix. I other words it assume that each group is covering a space of similar shape in the multidimensional space. This covariance **S** is then estimated by pooling the covariance matrices of each group:

$$s = \frac{1}{n-g}\sum_{1}^{g} n_i S_i \qquad \textbf{(Equation 5)}$$

Where *g* is the number of groups (here g =2), n_i and S_i are respectively the number of samples and the covariance of the group *i*. Similarly the mean values per group (μ_i) of the descriptors can be estimated on the training samples. Finally the probability of a given sample, characterized by its descriptors ***x*,** to belong to the group *i* can be evaluated using the Mahalanobis distance d_i:

$$d_i = (x-\mu_i)^T S^{-1} (x-\mu_i) \qquad \textbf{(Equation 6)}$$

The sample is then assigned to the group for which this distance is minimal. In order to compute this distance we need to invert the estimated covariance matrix **S**. This is only possible if **S** is of full rank which means that the data set contains necessarily more samples than descriptors. Note that the

discriminant function underlying this method is linear hence the boundary between the two groups is also linear.

3. Quadratic Discriminant Analysis - The assumption of common covariance is often not holding when dealing with biological data. This is one of the limits of LDA. Quadratic Discriminant Analysis[14] (QDA) is instead assuming a different covariance matrix for each group. This would correspond to groups presenting different shapes in the multidimensional space defined by the descriptors. The boundaries defined by QDA are not linear anymore but corresponds to (parts of) ellipses. The counterpart is that the number of samples per group must be superior to the number of descriptors to enable the inversion of each covariance matrix. Again each sample is assigned to the group that minimizes the Mahalanobis distance, but now using the difference $\mathbf{S}_i$:

$$d_i = (x - \mu_i)^T S_i^{-1} (x - \mu_i) \qquad \textbf{(Equation 7)}$$

4. Partial Least Squares Discriminant Analysis - Partial Least Squares Discriminant Analysis[17] (PLS-DA) is a classification method taking its roots into regression. Partial Least Squares was indeed firstly develop to regress a set of continuous descriptors **X** onto a continuous response **y**. The adaptation to classification method simply consists in replace the continuous response **y** by a binary version of it corresponding to the group label. PLS-DA constructs small number of latent variables, i.e. linear combinations of the descriptors, in order to capture most of the information present in both **X** and **y** and to maximize the covariance between the two matrices. The PLS-DA model can be summarized as follow:

$$y = X\beta + r \qquad \textbf{(Equation 8)}$$

Where β is the regression vector (comparable to the one discussed for the logistic regression) and **r** a vector of residuals.

5. Support Vector Machine - Support Vector Machines[14] (SVMs) are often considered as one of the most powerful classifier thanks to its ability to deal with non-linear problem, but it is also one of the most complex. The first step of this approach consists in mapping the samples into a new feature space using a Kernel transformation. A separating hyperplane is then defined in this new space based on few objects, the support vectors, close to the boundaries between the two groups. One drawback of the "kernel trick" is that the importance of the descriptor for the model is difficult to evaluate.[18,19]

2. SUPPLEMENTARY REFERENCES

1. Koopman, W. J. H. *et al.* Mitochondrial network complexity and pathological decrease in complex I activity are tightly correlated in isolated human complex I deficiency. *Am. J. Physiol. Cell Physiol.* **289,** C881–C890 (2005).
2. Distelmaier, F. *et al.* The antioxidant Trolox restores mitochondrial membrane potential and Ca^{2+} -stimulated ATP production in human complex I deficiency. *J. Mol. Med. (Berl).* **87,** 515–22 (2009).
3. Distelmaier, F. *et al.* Mitochondrial complex I deficiency: from organelle dysfunction to clinical disease. *Brain* **132,** 833–842 (2009).
4. Willems, P. H. G. M., Smeitink, J. A. M. & Koopman, W. J. H. Mitochondrial dynamics in human NADH:ubiquinone oxidoreductase deficiency. *Int. J. Biochem. Cell Biol.* **41,** 1773–1782 (2009).

5. Distelmaier, F. *et al.* Life cell quantification of mitochondrial membrane potential at the single organelle level. *Cytometry. A* **73,** 129–38 (2008).
6. Koopman, W. J. H. *et al.* Inhibition of complex I of the electron transport chain causes $O_2^{-\cdot}$ -mediated mitochondrial outgrowth. *Am. J. Physiol. Cell Physiol.* **288,** C1440–C1450 (2005).
7. Koopman, W. J. H., Visch, H., Smeitink, J. A. M. & Willems, P. H. G. M. Simultaneous Quantitative Measurement and Automated Analysis of Mitochondrial Morphology , Mass , Potential , and Motility in Living Human Skin Fibroblasts. *Cytom. Part A* **12,** 1–12 (2005).
8. Hoefs, S. J. G. *et al.* NDUFA2 Complex I Mutation Leads to Leigh Disease. 1306–1315 (2008). doi:10.1016/j.ajhg.2008.05.007.
9. Mortiboys, H. *et al.* Mitochondrial function and morphology are impaired in parkin-mutant fibroblasts. *Ann. Neurol.* **64,** 555–65 (2008).
10. Jonckheere, A. I. *et al.* Restoration of complex V deficiency caused by a novel deletion in the human TMEM70 gene normalizes mitochondrial morphology. *Mitochondrion* **11,** 954–963 (2011).
11. Valsecchi, F. *et al.* Primary fibroblasts of *NDUFS4*$^{-/-}$ mice display increased ROS levels and aberrant mitochondrial morphology. *Mitochondrion* **13,** 436–443 (2013).
12. Willems, P. *et al.* BOLA1 Is an Aerobic Protein That Prevents Mitochondrial Morphology Changes Induced by Glutathione Depletion. *Antioxid. Redox Signal.* 120911063348006 (2012). doi:10.1089/ars.2011.4253
13. De Groof, A. J. C. *et al.* The creatine kinase system is essential for optimal refill of the sarcoplasmic reticulum Ca2+ store in skeletal muscle. *J. Biol. Chem.* **277,** 5275–5284 (2002).
14. Hastie, T., Tibshirani, R. & Friedman, J. *The elements of statistical learning: data mining, inference and prediction*. *Springer Ser. Stat.* (Springer, 2001).
15. Peduzzi, P., Concato, J., Kemper, E., Holford, T. R. & Feinstem, A. R. A simulation study of the number of events per variable in logistic regression analysis. *J. Clin. Epidemiol.* **49,** 1373–1379 (1996).
16. Fisher, R. A. The use of multiple measurements in taxonomic problems. *Ann. Eugen.* **7,** 79–89 (1936).
17. Barker, M. & Rayens, W. Partial least squares for discrimination. *J. Chemom.* **17,** 166–173 (2003).
18. Krooshof, P. W. T., Ustun, B., Postma, G. J. & Buydens, L. M. C. Vizualization and recovery of the (Bio)chemical interesting variables in data analysis with support vector machine classification. *Anal. Chem.* **82,** 7000–7007 (2010).
19. Smolinska, A. *et al.* Interpretation and visualization of non-linear data fusion in kernel space: study on metabolomic characterization of progression of Multiple Sclerosis. *PLoS One* **7,** e38163 (2012).

A

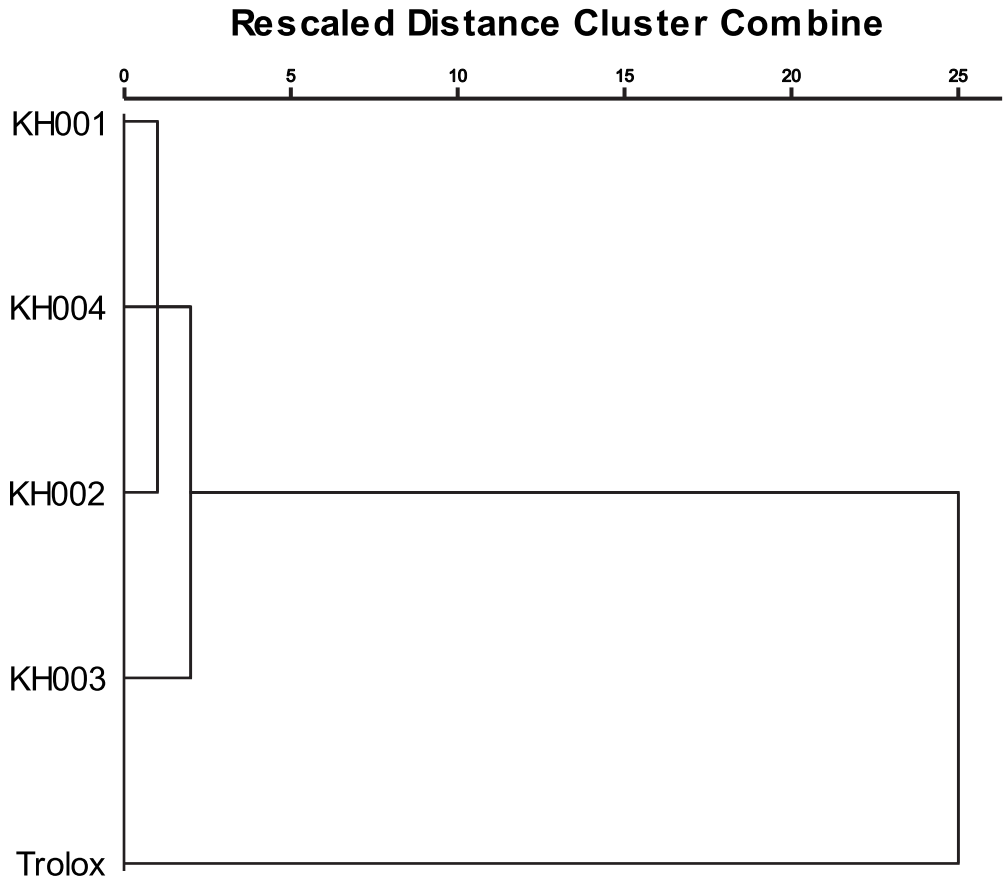

B

Proximity Matrix

Case	Trolox	KH001	KH002	KH003	KH004
Trolox	.000	77483.520	83003.453	53089.685	88442.581
KH001	77483.520	.000	1104.169	2531.015	480.495
KH002	83003.453	1104.169	.000	3626.391	1785.468
KH003	53089.685	2531.015	3626.391	.000	4983.220
KH004	88442.581	480.495	1785.468	4983.220	.000

Figure S1: Physicochemical similarity between Trolox and its newly developed variants. (**A**) Dendrogram obtained by cluster analysis of the predicted physicochemical parameters for Trolox, KH001, KH002, KH003 and KH004 (Supplementary Table S3). (**B**) Proximity matrix based upon panel A. Lower numbers indicate a greater similarity between compounds.

Table S1: Definition of mitochondrial descriptors and values in vehicle- and compound-treated patient cells.

#	Descriptor[a]	Definition[b]	P5175[f]	Trolox[f]	KH001[f]	KH002[f]	KH003[f]	KH004[f]
1	**Area polygon** (O)	The area of the polygon that defines the object's outline	**0.89**	**1.07**	1.00	**1.03**	**1.13**	1.02
2	**AreaOnBox** (O)	Reports the ratio between the area of an object and the area of its bounding box	**1.06**	0.98	0.98	0.99	**0.94**	**0.97**
3	**Aspect**[d] (O)	Ratio between major axis and minor axis of ellipse equivalent to object (a.k.a. Aspect Ratio or *AR*)	**0.89**	**0.96**	**0.95**	**0.96**	**1.03**	0.98
4	**Axis minor** (O)	Length of minor axis of ellipse with same moments of order 1 and 2 as object	1.01	**1.03**	1.02	1.03	1.02	1.02
5	**Box XonY** (O)	Ratio between width and height of object's bounding box	1.00	1.00	1.03	0.99	1.01	0.98
6	**Box height** (O)	Height of the object's bounding box	**0.92**	**1.04**	0.99	1.01	**1.09**	**1.05**
7	**Box width** (O)	Width of the object's bounding box	**0.93**	**1.04**	**1.03**	1.01	**1.09**	1.00?
8	**Count** (P)	Size weighted object "count"	1.00	1.00	1.00	1.00	1.00	1.00
9	**Density max** (O)	Maximum intensity or density inside object	**0.86**	**0.76**	**0.75**	**0.75**	**0.85**	**0.75**
10	**Density mean** (O)	Average optical density (or intensity) of object	**0.86**	**0.73**	**0.72**	**0.74**	**0.82**	**0.73**
11	**Density min** (O)	Minimum intensity or density inside object	**0.87**	**0.67**	**0.69**	**0.71**	**0.75**	**0.69**
12	**Density std dev** (O)	Standard deviation of intensity or density inside object	**0.87**	**0.81**	**0.77**	**0.77**	**0.92**	**0.79**
13	**Diameter max** (O)	Length of longest line joining two points of object's outline and passing through the object's centroid	**0.91**	1.01	1.00	1.00	**1.06**	1.00
14	**Diameter mean** (O)	Average length of diameters measured at 2 degree intervals and passing through the object's centroid	**0.94**	1.02	1.00	1.00	**1.06**	1.01
15	**Diameter min** (O)	Length of shortest line joining two points of object's outline and passing through the object's centroid	1.00	1.02	1.01	1.02	1.03	1.01
16	**Feret max**[c] (O)	Longest feret (caliper) length	**0.88**	1.03	1.00	1.00	**1.11**	1.02
17	**Feret mean**[c] (O)	Average feret (caliper) length	**0.91**	**1.03**	1.00	1.01	**1.09**	1.02
18	**Feret min**[c] (O)	Smallest feret (caliper) length	0.99	**1.06**	1.03	**1.04**	**1.05**	1.03
19	**IOD** (P)	Integrated optical density of all objects	**0.78**	**0.75**	**0.70**	**0.75**	**0.90**	**0.73**
20	**Length** (O)	Feret diameter (caliper length) along the major axis of the object	**0.88**	1.03	1.00	1.00	**1.11**	1.02
21	**Margination**[e] (O)	The distribution of intensity between the center of an object and the edge of the object.	1.00	0.99	0.99	0.98	0.99	0.98
22	**Perimeter** (O)	Length of the object's outline.	**0.90**	**1.04**	1.00	1.01	**1.10**	1.03
23	**Perimeter convex** (O)	Perimeter of the convex outline of the object	**0.90**	**1.04**	1.00	1.01	**1.10**	1.02
24	**Perimeter ellipse** (O)	The perimeter of the ellipse surrounding the outline of each object.	**0.91**	1.03	0.99	1.00	**1.08**	1.02
25	**Perimeter ratio** (O)	Ratio of convex perimeter to perimeter	1.00	0.99	0.99	1.00	1.00	0.99
26	**Perimeter2** (O)	Chain code length of the outline	**0.90**	**1.04**	1.00	1.01	**1.10**	1.03
27	**Radius max** (O)	Minimum distance between object's centroid and outline	**0.88**	**1.03**	1.00	1.01	**1.11**	1.03
28	**Radius min** (O)	Maximum distance between object's centroid and outline	**1.06**	**1.03**	1.02	1.02	1.00	1.01
29	**Radius ratio** (O)	Ratio between descriptors "Radius max" and "Radius min"	**0.81**	**1.03**	**1.03**	1.01	**1.19**	**1.06**
30	**Roundness**[d] (O)	$Perimeter^2/(4*\pi*Area$; a.k.a. Formfactor or *F*)	**0.91**	1.02	1.01	1.01	**1.09**	**1.06**
31	**Width** (O)	Feret diameter (caliper length) along the minor axis of the object	1.00	**1.06**	**1.03**	**1.04**	**1.05**	**1.04**

[a]The descriptor reports on individual mitochondrial objects (O) or on the population (P) of all objects in each image. [b]As defined in the Image Pro Plus analysis software. [c]Feret is a measure of object size along a specified direction. [d]A value of 1.0 for this parameter represents a perfect circle. [e]A value of 0.33 for this parameter indicates an object with a homogeneous intensity distribution. [f]The number reflects the descriptor ratio value (P5175/CT5120) in vehicle-treated fibroblasts, based upon median descriptor values per image. Numbers in **bold** represent significant changes in this ratio ($p<0.05$; red depicts an increased, blue depicts a decrease).

Table S2: Performance of the various machine learning algorithms.

CLASSIFICATION ALGORITHM	DATASET USED FOR ANALYSIS		
	All data[a]	**Mean[b]**	**Median[b]**
Logistic Regression (LogReg)	63.86	78.10	78.95
Linear Discriminant Analysis (LDA)	57,35	77.42	76.40
Partial Least Squares Discriminant Analysis (PLSDA)	N.d.	64.86	65.36
Quadratic Discriminant Analysis (QDA)	61.98	71.82	70.63
Support Vector Machine (SVM; sigma = 30)	N.d.	75.72	77.42

The number reflects the percentage of correctly classified P5175 (patient) cells relative to CT5120 (control) cells for the different classification algorithms using the 31 mitochondrial descriptors.

[a]Calculated for individual mitochondrial objects.

[b]Calculated using the mean or median value of each individual image (CT)

Abbreviations: N.d., values not determined due to the numerical complexity of these models.

Table S3: Predicted physicochemical properties and biochemical and cellular effects of Trolox and its derivatives.

Parameter	Trolox	KH001	KH002	KH003	KH004
Physicochemical properties					
MW	250.29	392.47	391.48	365.44	407.48
LogP	3.66	0.84	1.12	2.55	2.21
LogD	0.38	-1.53	-1.25	0.28	0.57
POL	25.29	42.85	42.45	39.24	43.49
DM	3.65	40.78	40.52	39.53	42.61
tPSA	69.59	151.3	125.28	126.33	162.33
MSA	391.47	612.14	632.6	578.71	622.02
PI	N.a.	10.9	10.9	6.61	7.18
pKa	10.8	10.36	10.75	10.72	10.55
DC	1	6	5	3	5
DS	1	8	6	5	7
AC	4	6	5	5	7
AS	9	10	9	11	13
Biochemical and cellular effects					
ORAC	1.000 (R=0.999)	0.933 (R=0.990)	0.835 (R=0.991)	1.053 (R=0.996)	0.438 (R=0.999)
DCFDA	**P5175:** 0.77±0.06* **P5866:** 0.90±0.05* **P6173:** 0.67±0.15* **P6603:** 0.94±0.07	**P5175:** 0.73± 0.12*	**P5175:** 1.01±0.11 **P5866:** 0.90±0.06* **P6173:** 0.72±0.08* **P6603:** 0.82±0.07*	**P5067:** 0.74±0.06* **P5175:** 0.70±0.10* **P5260:** 0.92± 0.08 **P5866:** 0.77±0.10* **P6603:** 0.74±0.11* **P6173:** 0.74±0.12*	**P5175:** 0.78±0.11*
HEt	**P5175:** 0.95±0.01	**P5175:** 1.11±0.04*	**P5175:** 0.76±0.02*	**P5175:** 0.87±0.02*	**P5175:** 0.96±0.06
CI activity	**CT5120:** 1.59±0.10* **P7206:** 1.50±0.06*	**CT5120:** 1.69 (n=2) **P7206:** 1.01 (n=2)	**CT5120:** 1.30 (n=2) **P7206:** 0.61 (n=2)	**CT5120:** 1.53 (n=2) **P7206:** 1.67 (n=2)	**CT5120:** 1.65 (n=2) **P7206:** 1.33 (n=2)
CIV activity	**CT5120:** 1.74±0.09* **P7206:** 1.67±0.06*	**CT5120:** 1.68 (n=2) **P7206:** 1.29 (n=2)	**CT5120:** 1.55 (n=2) **P7206:** 0.95 (n=2)	**CT5120:** 1.58 (n=2) **P7206:** 1.51 (n=2)	**CT5120:** 1.74 (n=2) **P7206:** 1.05 (n=2)
CS activity	**CT5120:** 1.57±0.07* **P7206:** 1.42± 0.08*	**CT5120:** 1.36 (n=2) **P7206:** 1.38 (n=2)	**CT5120:** 1.70 (n=2) **P7206:** 0.75 (n=2)	**CT5120:** 1.67 (n=2) **P7206:** 1.38 (n=2)	**CT5120:** 1.52 (n=2) **P7206:** 1.09 (n=2)

All physicochemical properties in this table were calculated using MarvinSketch 6.1.3 software (ChemAxon Ltd., Budapest, Hungary) using default settings unless stated otherwise (N.a., not appropriate).

Statistics: *($p<0.05$).

Abbreviations: AC, hydrogen bond acceptor count of major microspecies at pH 7.4; AS, hydrogen bond acceptor sites of major microspecies at pH 7.4. CI, CIV, CS enzymatic activities, effect on biochemical activity of complex I (CI), complex IV (CIV) and citrate synthase (CS) in mitochondria-enriched fractions of CT5120 and P7206 cells. Each activity value reflects the average of two measurements and is expressed as the ratio between treated/vehicle-treated condition (in mU/mg). For P7206 the vehicle-treated activity values (mU/mg protein as percentage of CT5120) were: 30% (CI) 87% (CIV) and 118% (CS). Treatment duration was 96 h and a 500 µM concentration was used for each compound; DC, hydrogen bond donor count for major microspecies at pH 7.4; DCFDA: Values were calculated from 16 replicate wells in 4 independent experiments and expressed as treated/vehicle-treated condition; DS, hydrogen bond donor sites for major microspecies at pH 7.4; DM, dipole moment in Debye, a measure of net molecular polarity; MSA, molecular surface area (van der Waals surface) in $Å^2$; MW, molecular weight in g/mol; HEt, effect of compound treatment (500 µM; 72 h incubation) on HEt oxidation. Values were calculated from 16 replicate wells in 4 independent experiments and expressed as treated/vehicle-treated condition; LogP, octanol/water partition coefficient (non-ionic species); LogD, octanol/water distribution coefficient at pH 7.4; ORAC, oxygen radical absorbance capacity; pKa, pKa-value of the chroman hydroxyl (antioxidant) group; PI, isoelectric point, the pH at which the molecule has a net charge of zero; POL, polarizability in $Å^3$; tPSA, topological polar surface area in $Å^2$ a parameter shown to correlate very well with the human intestinal absorption, Caco-2 monolayers permeability, and blood-brain barrier penetration. This value was calculated for the major microspecies at pH 7.4.